FLUXFORMER: UPSCALED GLOBAL CARBON FLUXES FROM EDDY COVARIANCE DATA WITH MULTIVARIATE TIMESERIES TRANSFORMER

A NON-PEER REVIEWED PREPRINT. LATER VERSIONS OF THIS PAPER MAY INCLUDE REVISIONS AND UPDATES.

Anh Phan [*1] **and Hiromichi Fukui** [† 2,3]
[1]Graduate School of Engineering, Chubu University, Kasugai, Japan
[2]Chubu Institute for Advanced Studies, Chubu University, Kasugai, Japan
[3]International Digital Earth Applied Science Research Center (IDEAS), Chubu University, Kasugai, Japan

December 5, 2023

ABSTRACT

We provided a monthly global gross primary production (GPP) and ecosystem respiration (RECO) dataset from 1990 to 2019 at 0.25° × 0.25° spatial resolution named FluxFormer by utilizing the new plant function type dataset in combination with multivariate timeseries Transformer-based model. FluxFormer outperforms other satellite-derived upscaled products when comparing the correlation at site-level and seasonal pattern with FLUXNET 2015, especially in tropical regions. Additionally, our dataset shows the highest positive trend in GPP from 2001 to 2019, aligning with trends derived from dynamic global vegetation models that account for the CO_2 fertilization effect. Notably, FluxFormer captures positive long-term trends that are not replicated by some existing products. FluxFormer could be used to validate terrestrial biosphere models and serve as a tool for cross-checking other datasets. The FluxFormer GPP and RECO product is available at `https://doi.org/10.5281/zenodo.10258644`.

Keywords Transformer · Gross primary production · Ecosystem respiration · Plant functional type

1 Introduction

Terrestrial ecosystems play a crucial role in mitigating global warming by serving as a persistent carbon sink, actively absorbing and storing excess carbon dioxide from the atmosphere [Pan et al., 2011]. Over the period from 2010 to 2019, the terrestrial CO_2 sink is estimated to offset fossil CO_2 emissions by 35%, surpassing the ocean, which is projected to remove 26% of fossil-fuel-derived CO_2 [Friedlingstein et al., 2020, Wang et al., 2022]. The substantial global carbon flux, known as terrestrial gross primary production (GPP), significantly contributes to the reduction of anthropogenic CO_2 emissions [Beer et al., 2010].

Estimating GPP involves various methods, such as simulating dynamic global vegetation models (DGVMs) like those employed in the TRENDY project [Sitch et al., 2015, Le Quéré et al., 2018], upscaling from measurements obtained through eddy covariance (EC) flux tower and satellite observations [Jung et al., 2019, Zeng et al., 2020]. However, all these approaches rely on plant functional types (PFTs) to estimate ecosystem productivity [Poulter et al., 2011, 2015, Lin et al., 2021, Guo et al., 2023, Yan et al., 2023]. Inconsistencies in PFT maps can significantly contribute to uncertainties in GPP estimations, as well as other climate-relevant variables, at both regional and global scales [Poulter et al., 2011]. Particularly in the tropical region, the sparse distribution of EC sites, the high species richness of trees, and the complex vertical structure of tropical rainforests pose challenges [Montgomery and Chazdon, 2001], making it difficult to accurately quantify the seasonality of carbon fluxes [Xu et al., 2015].

[*]`anhphancu@gmail.com`
[†]`fukui@isc.chubu.ac.jp, hiromichi.fukui@gmail.com`

In recent times, there has been an increasing adoption of timeseries (TS) foundation models employing a transformer-inspired architecture for addressing timeseries problems and representation learning. Notable examples include the MVTS Transformer [Zerveas et al., 2021], Informer [Zhou et al., 2021], Autoformer [Wu et al., 2021], and Fedformer [Zhou et al., 2022]. The adoption of the Transformer architecture is anticipated to enhance the modeling of seasonality based on the timeseries representation. However, to the best of our knowledge, its application in the task of upscaling global carbon fluxes remains limited.

In this section, our goal is to evaluate the effectiveness of employing timeseries representation, specifically based on recently updated Plant Functional Types (PFTs) [Harper et al., 2022] and a Transformer-based architecture model [Zerveas et al., 2021], for predicting the trends and seasonality of carbon fluxes at a global scale. We present monthly global data at a spatial resolution of 0.25 degrees for GPP and Ecosystem Respiration (RECO). The evaluation of our dataset involves comparing it with other satellite-based carbon flux datasets, considering correlations with FLUXNET 2015 and Solar-Induced Fluorescence (SIF) datasets, as well as assessing interannual trends and variations. The complete workflow of the study is illustrated in Figure 1, and we have named our dataset and framework FluxFormer.

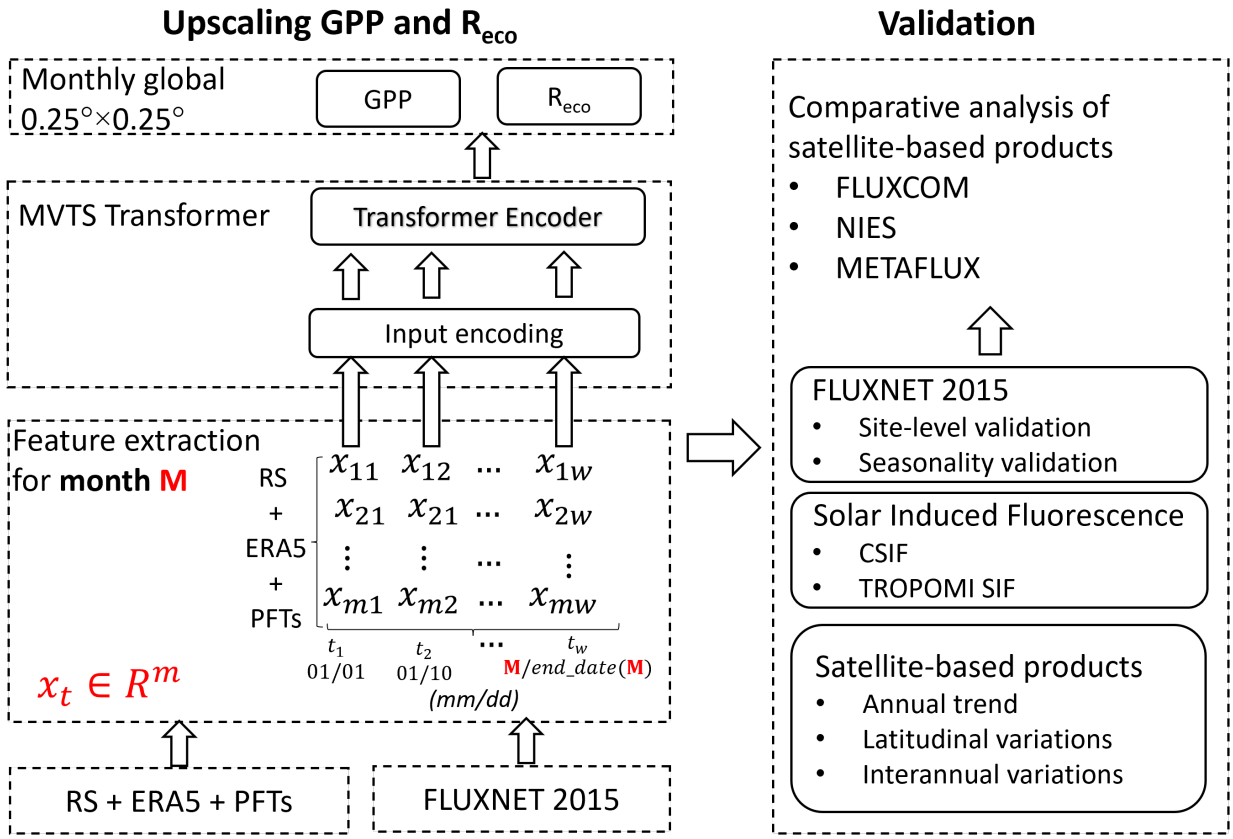

Figure 1: Schemantic workflow of our FluxFormer methodology

2 Method

2.1 Input data

2.1.1 FLUXNET 2015

The FLUXNET 2015 dataset [Pastorello et al., 2020] serves as the groundtruth for carbon fluxes in the transformer model in this study. Monthly GPP and RECO data were extracted from the dataset tier 1 of FLUXNET 2015, encompassing data from 206 sites. We filtered out records with a quality control value of less than 80% for measured and good-quality gap-fill data. Relying solely on quality control values is reported to be insufficient for obtaining qualified data due to inconsistencies in the differences between GPP, RECO, and NEE [Zeng et al., 2020, Tramontana et al., 2016]. Following

the approach of [Zeng et al., 2020], we also excluded records with an absolute difference between GPP-RECO and NEE larger than 0.1 gC $m^{-2}d^{-1}$.

2.1.2 Remote sensing data

For the remote sensing data, we employed version 2 of the global leaf area index (LAI) and fraction of absorbed photosynthetically active radiation (FAPAR) datasets, generated using the algorithm proposed by [Verger et al., 2014]. These datasets can be accessed through the Copernicus Global Land Service, providing a 1 km spatial resolution for every 10 days spanning from 1999 to 2019. The remote sensing data utilized in this study is in line with the approach presented in [Zeng et al., 2020]. The latitude boundary of this dataset ranges from -60°S to 80°N.

2.1.3 Meteorological data

For meteorological data, we employed specific variables from the ERA5 reanalysis product [Hersbach et al., 2020], including 2-meter air temperature (T2M), surface short-wave (solar) radiation downwards (SSRD), vapor pressure deficit (VPD), total precipitation (TP), and evaporation (E). As VPD is not directly available in the original dataset, we estimated it using the relationship between saturated vapor pressure (SVP) and actual vapor pressure (AVP): VPD = SVP - AVP, based on 2-meter air and dewpoint temperature. The original spatial resolution of ERA5 data is 0.25° × 0.25° and was obtained from the Copernicus Climate Change Service (C3S) Climate Data Store (CDS).

2.1.4 Plant function types

The PFTs dataset employed in this study, denoted as PFT v2.0.8 and obtained from [Harper et al., 2022], spans the period from 1992 to 2020. It provides the specific percentage cover of 14 PFTs for each pixel at a 300m resolution. The annual dataset comprises 14 layers, with pixel values at 300m resolution indicating the percentage cover (ranging from 0% to 100%) for each of the 14 PFTs. This updated PFTs dataset is considered a more accurate representation of PFT distributions as it relies on high-resolution, peer-reviewed mapping of specific vegetation classes to refine global assumptions about PFT fractions [Harper et al., 2022]. Regional updates in PFT fractions are anticipated to enhance carbon fluxes estimation. The complete set of PFTs includes bare soil, built areas, water bodies, snow and ice, natural grasses, managed grasses (i.e., herbaceous cropland), broadleaved deciduous trees, broadleaved evergreen trees, needleleaved deciduous trees, needleleaved evergreen trees, broadleaved deciduous shrubs, broadleaved evergreen shrubs, needleleaved deciduous shrubs, and needleleaved evergreen shrubs. The dataset can be accessed from the CEDA archive at https://catalogue.ceda.ac.uk/uuid/26a0f46c95ee4c29b5c650b129aab788.

2.2 Multivariate Time Series Transformer Framework

Figure 1 illustrates the overall workflow of our FluxFormer methodology to upscale GPP and RECO from remote sensing data, and PFTs data. We utlized the original Multivariate Time Series MVTS Transformer model which is transformer-based framework proposed by [Zerveas et al., 2021] which contains an input encoding layer with learnable positional encoding and a Transformer Encoder [Vaswani et al., 2017]. MVTS Transformer achieved good performance on supervised and unsupervised regression task based on multivariate time series representation even with limited training samples.

In order to train the MVTS Transformer, first, we extracted the remote sensing data, meteorological data and PFTs for each monthly record from FLUXNET 2015 dataset. Then the extracted data is formed to feed to the deep learning model. In particular, for a specific month **M**, each traing sample $\mathbf{X} \in \mathbb{R}^{w \times n}$ where *w* is the lengths of timeseries for month **M** ($w = 3 \times \mathbf{M}$ as we have three remote sensing products per month) and *m* is the number of different variables ($m = 21$: 2 remote sensing varibales (LAI and FAPAR), 5 meteorological variables (T2M, SSRD, VPD, TP, E) and 14 PFTs variables), constitutes a sequence of *w* feature vectors $\mathbf{x}_t \in \mathbb{R}^m : \mathbf{X} \in \mathbb{R}^{w \times n} = [\mathbf{x}_1, \mathbf{x}_1, \ldots, \mathbf{x}_w]$ is a multivariate timeseries of length *w* and *m* different variables.

2.3 Training setup

To train the model, approximately 80% of the monthly data was randomly chosen for training, while the remaining 20% was allocated for validation. Twelve models were trained over the course of 12 months.

Notably, the distribution of FLUXNET 2015 sites is uneven across climate zones, particularly in the tropics and semi-arid regions, despite the highest GPP values being observed in tropical areas such as Amazonia, Central Africa, and Southeast Asia [Chen et al., 2017]. Additionally, semi-arid regions play a crucial role in influencing the global carbon cycle [Poulter et al., 2014]. To reduce this imbalance, we exclusively utilized the most recent data from the past three years for each site as suggested by [Zeng et al., 2020]. This choice aimed to guarantee a fairer representation

Table 1: Number of samples for training and validation

	Number of samples	
Month	Training	Validation
January	363	68
February	377	72
March	392	77
April	385	75
May	408	88
June	372	66
July	379	66
August	365	67
September	387	68
October	406	71
November	385	75
December	357	62

of each site during the training of the transformer model. This approach yielded a total of 4576 samples over the 12-month period, derived from the pool of 10655 qualified monthly samples. The distribution of samples for training and validation is outlined in Table 1.

2.4 Validation

To evaluate our product's quality, we performed a comparative analysis against other remote sensing-based products, including FLUXCOM [Jung et al., 2019], NIES [Zeng et al., 2020], and MetaFlux [Nathaniel et al., 2023]. Initially, we assessed the correlation of monthly FLUXNET 2015 GPP and RECO values with the corresponding data from these products at the FLUXNET sites. Additionally, we examined the seasonality trends in our data across climate zones in comparison to FLUXNET 2015.

Following that, we carried out a seasonality analysis utilizing SIF data from two distinct SIF products: CSIF [Zhang et al., 2018] (available at `https://fgshare.com/articles/dataset/CSIF/6387494`) and TROPOMI SIF [Köhler et al., 2018] (accessible via `ftp://fluo.gps.caltech.edu/data/tropomi/`).

Ultimately, we examined the interannual trends and variations, as well as the latitudinal patterns of our outputs in comparison with FLUXCOM, NIES, and MetaFlux. To evaluate interannual trends, we computed the annual global mean GPP and RECO, scaling the global average fluxes using the total global land area of 122.4 million square kilometers from [Friedl et al., 2010], as recommended by [Jung et al., 2020] to ensure consistent global area representation across all products. The annual trends and their statistical significance in GPP and RECO were indicated by the slope of the linear regression line and the corresponding p-value. For the assessment of interannual variations, we determined the Interannual Variability (IAV) at the pixel level by calculating the standard deviation divided by the mean of annual fluxes.

3 Data records

We provided global monthly data of GPP and RECO available at 0.25-degree spatial resolution. The latitude boundary extends from -60°S to 80°N which is same as the latitude boundary of the remote sensing used in this study. The longitude extends from -180°W to 180°S. The data is provided in Network Common Data Form (NetCDF) format. The data variables are defined by time, latitude, longitude coordinates. In the provided data, we purposely masked out the cold regions that consist of the Arctic circle and the desert region.

We show an example of our GPP in Figure 2a and RECO in Figure 2b in comparison with other selected satellite-based upscaled products. We can observed that despite the uncertainties between the products, highest GPP and RECO values in tropical regions and lowest values in the semi-arid regions in all products.

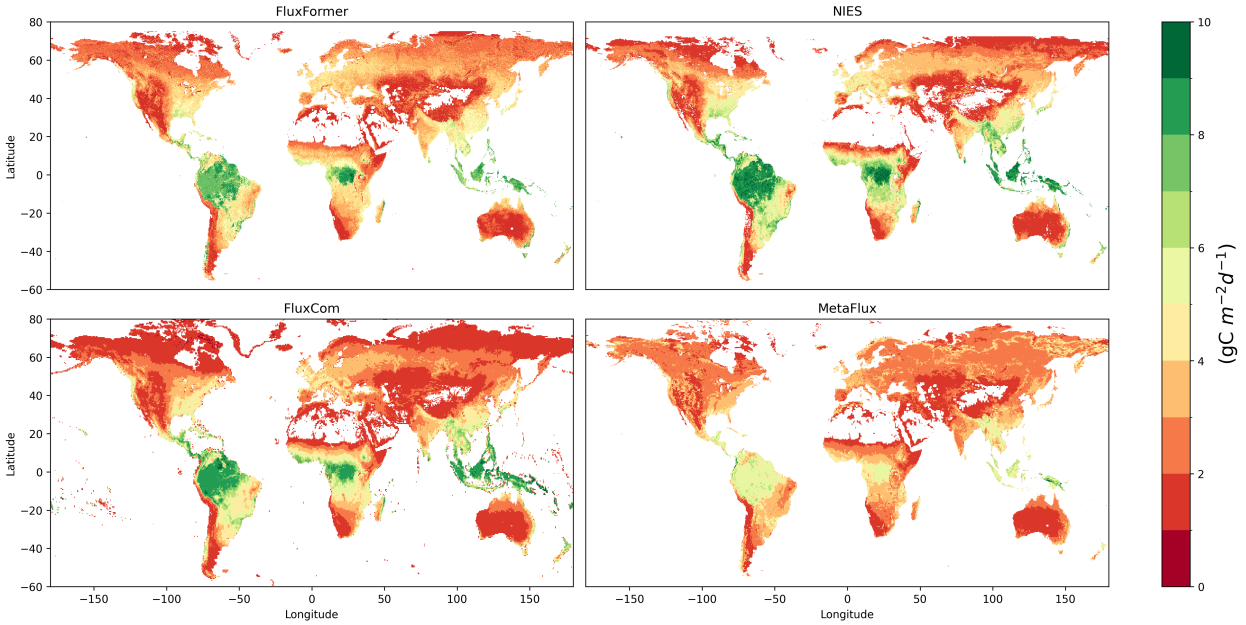

(a) GPP

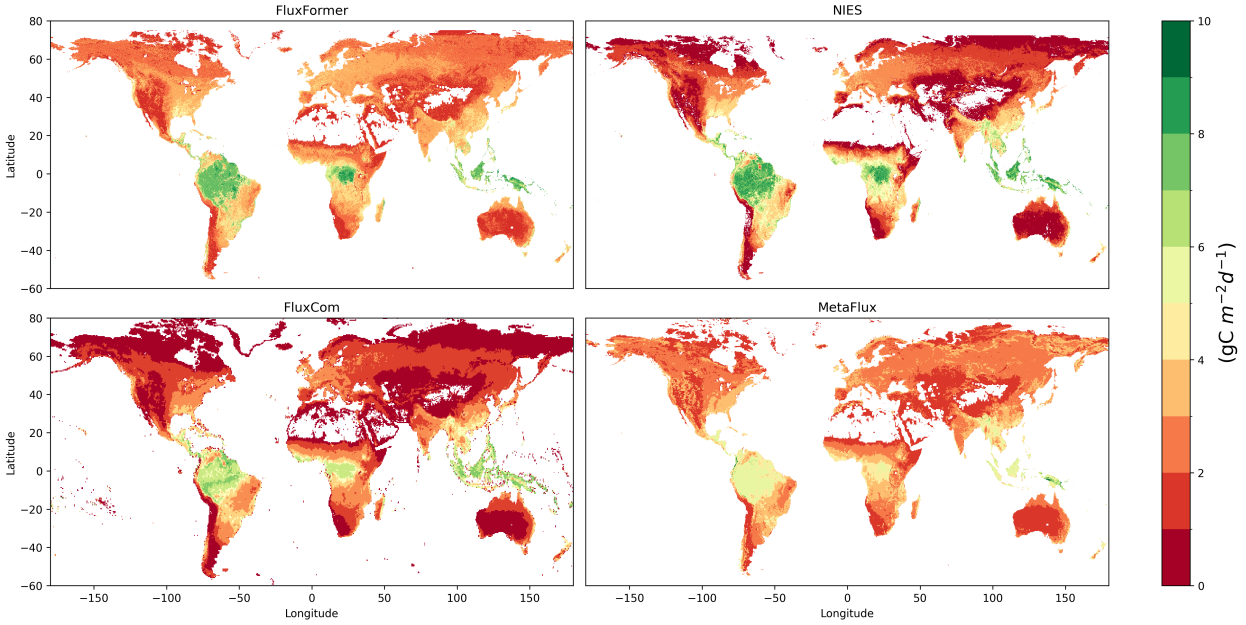

(b) RECO

Figure 2: Mean estimate of (a) GPP and (b) RECO for the year 2017: GPP (a) RECO (b)

4 Technical validation

4.1 Validation with FLUXNET 2015

4.1.1 Site-level validation

We utilized the Pearson Correlation Coefficient (R) and Root Mean Square Error (RMSE) to assess the quality of our products in comparison to FLUXNET 2015 observations. As depicted in Figures 3a and 3b, our product demonstrates the highest correlation and the lowest RMSE with FLUXNET 2015 for both GPP and RECO data ($R = 0.894, RMSE = 1.706$ for GPP and $R = 0.866, RMSE = 1.244$ for RECO). In contrast, MetaFlux shows the lowest correlation with

FLUXNET 2015 ($R = 0.652, RMSE = 3.135$ for GPP and $R = 0.612, RMSE = 2.046$ for RECO). NIES and FLUXCOM also exhibit strong correlations with the ground truth data, achieving $R/RMSE : 0.857/1.981$ (NIES), $0.819/2.32$ (FLUXCOM) for GPP and $R/RMSE : 0.795/1.511$ (NIES), $0.792/1.627$ (FLUXCOM) for RECO.

4.1.2 Seasonality validation

We analyzed the seasonal trend using FLUXNET 2015 data, calculating monthly mean values across climate zones, as depicted in Figure 4 and Table 2. In arid regions, FluxFormer, FluxCom, and NIES exhibited high correlation ($R > 0.9$) with FLUXNET for both GPP and RECO. However, MetaFlux showed lower correlation with $R = 0.48$ for GPP and $R = 0.66$ for RECO in arid regions. For temperate and cold regions, all satellite-based products (FluxFormer, FLUXCOM, NIES, and MetaFlux) demonstrated high correlations ($R > 0.97$) with FLUXNET 2015 GPP and RECO.

Table 2: Pearson correlation of seasonal trend with FLUXNET 2015

Climate groups	FluxFormer	FluxCom	NIES	MetaFlux
GPP				
Arid	0.91	0.91	0.94	0.48
Temperate	0.99	0.99	0.97	0.97
Cold	1	0.99	1	0.99
Trop. SVN	0.99	0.99	0.94	0.97
Trop. MS	**0.84**	0.04	0.58	-0.05
Trop. RF	0.68	0.6	0.71	0.41
RECO				
Arid	0.94	0.92	0.95	0.66
Temperate	0.98	0.99	0.99	0.99
Cold	1	0.99	1	1
Trop. SVN	0.99	0.98	0.92	0.91
Trop. MS	**0.88**	0.51	0.29	0
Trop. RF	**0.68**	0.37	0.5	0.47

In the tropical region, we partitioned the area into tropical savanna (Trop. SVN), tropical monsoon (Trop. MS), and tropical rainforest (Trop. RF). In Trop. SVN, all satellite-based products displayed a high correlation with FLUXNET 2015 for both GPP and RECO. Conversely, for Trop. MS, our data exhibited the highest correlation at $R = 0.84$, while NIES data showed a moderate correlation ($R = 0.58$). FLUXCOM and MetaFlux demonstrated no correlation with FLUXNET 2015 for GPP, with $R < 0.1$. Regarding RECO in Trop. SVN, our data maintained the highest correlation with the seasonal trend of the ground truth, whereas other products showed lower correlation (FLUXCOM: $R = 0.51$, NIES: $R = 0.29$) or no correlation with the ground truth (MetaFlux: $R = 0$). In the Trop. RF area, our data exhibited the second-highest correlation with GPP seasonal trend ($R = 0.68$) and the highest correlation with RECO seasonal trend ($R = 0.68$).

Overall, our data demonstrates a robust correlation in arid, temperate, cold, and Trop. SVN regions, surpassing $R > 0.9$ for both GPP and RECO. Specifically, in Trop. MS, our data exhibits the highest correlation, reaching $R = 0.84$ for GPP and $R = 0.88$ for RECO. In the Trop. RF region, our data exhibits the second-highest correlation with the ground truth GPP seasonal trend ($R = 0.68$) and the highest correlation with the ground truth RECO seasonal trend ($R = 0.68$) among the selected satellite-based products.

4.2 Validation with SIF

SIF serves as a reliable proxy and has seen increased usage for estimating GPP [Norton et al., 2019, Liu et al., 2020, Bai et al., 2022]. To expand the seasonality validation, we incorporated independent products, namely CSIF and TROPOMI SIF. We examined the pixel-level correlation distribution of FluxFormer and selected satellite-based products with the seasonal trend of CSIF from 2000 to 2019 and TROPOMI SIF from 2018 to 2019, as TROPOMI data is available only from 2018 onwards.

Previous studies generally assumed that linear relationship between GPP and SIF [Guanter et al., 2012, Yang et al., 2017]. However this assumptions across climate regions and PFTs remains uncertains [Gu et al., 2019, Xiao et al., 2019, Zhang et al., 2016, Chen et al., 2021] especially in tropical regions where the evidents from showing that weak or no relationships of GPP with SIF in there as well as in South America and in subtropical Africa [Doughty et al., 2021]. The results are illustrated in Figure 5a and Figure 5b. We observed that our data exhibits lower correlation with CSIF and TROPOMI SIF in tropical regions (Central and South America, West and Central Africa, and Southeast Asia) and

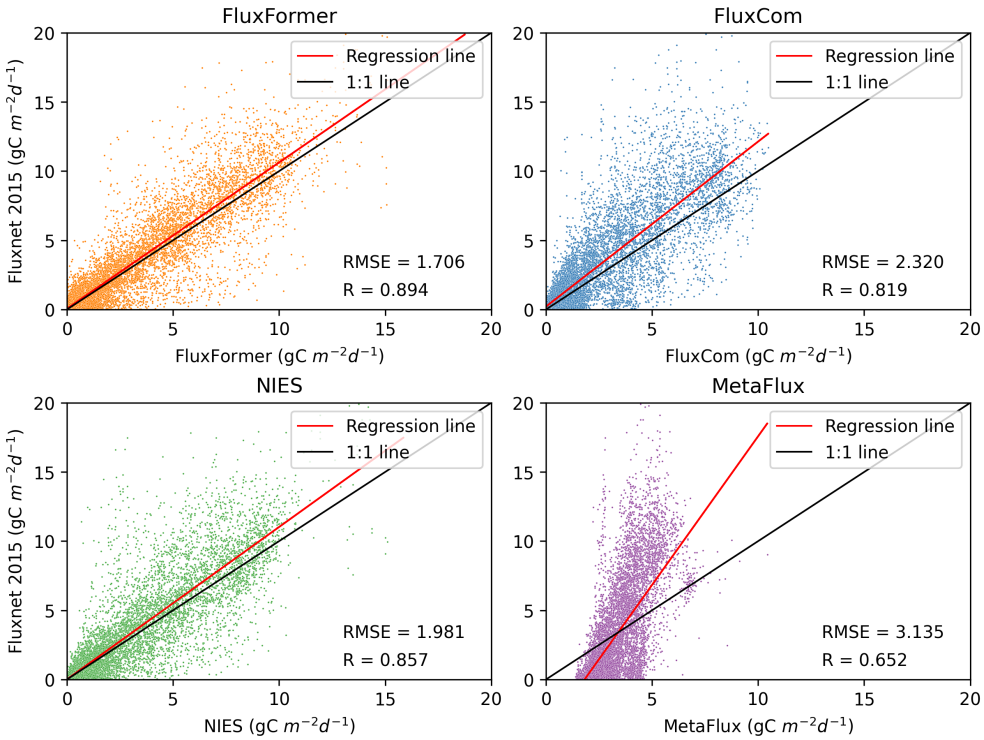

(a) GPP

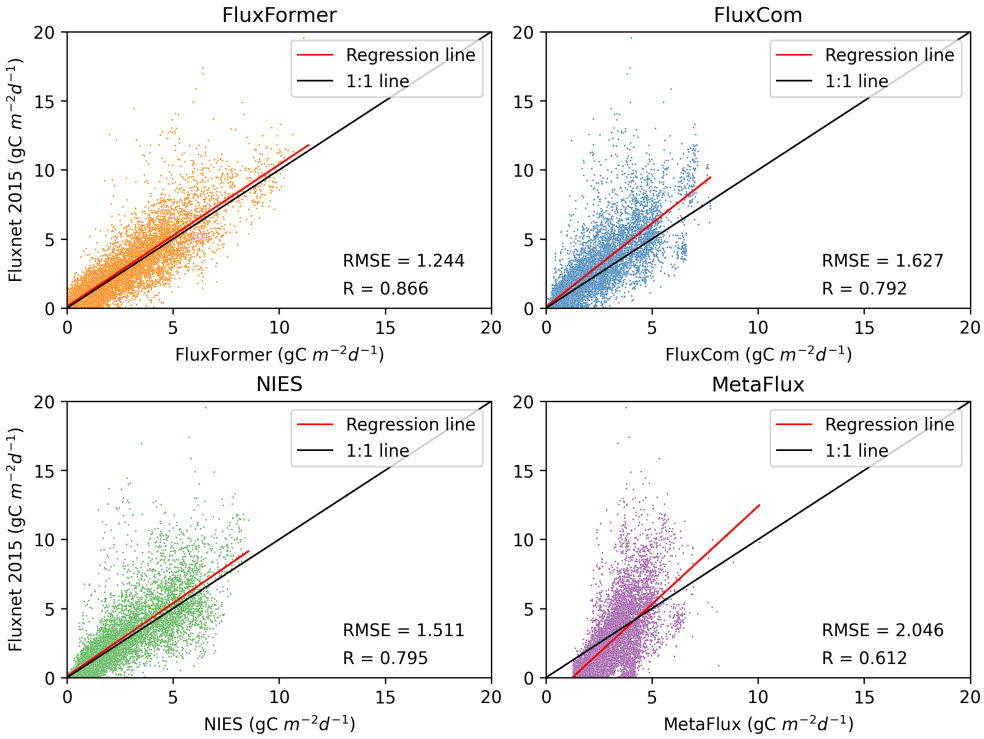

(b) RECO

Figure 3: Validation with FLUXNET 2015: GPP (a) RECO (b)

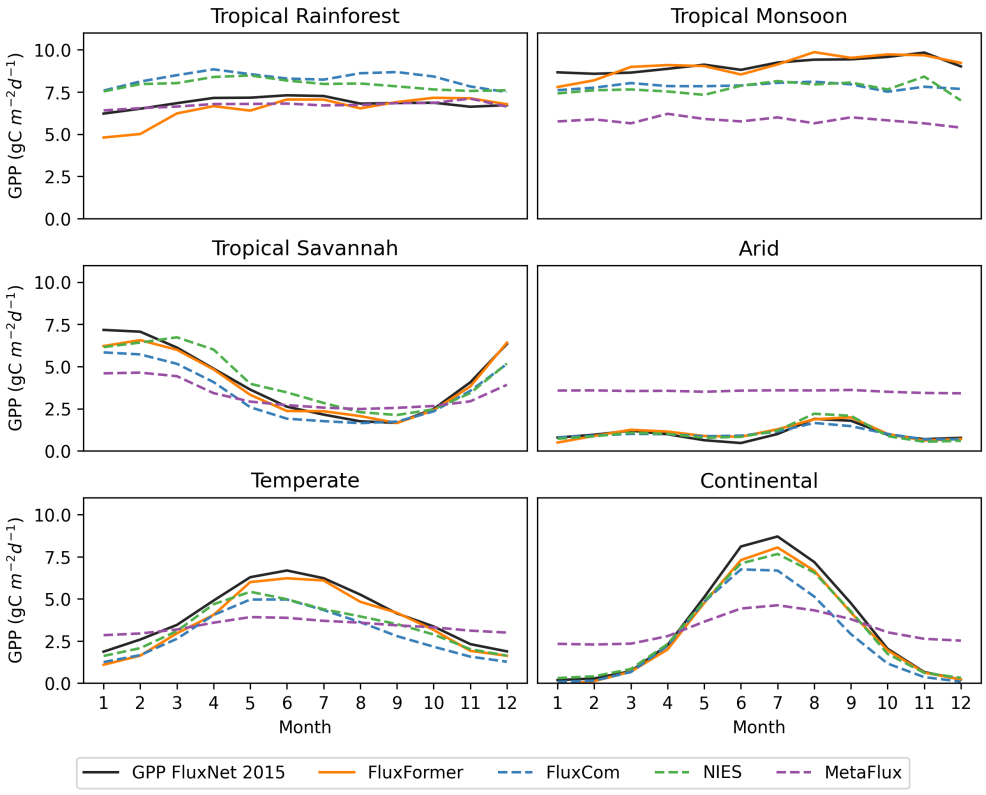

(a) GPP

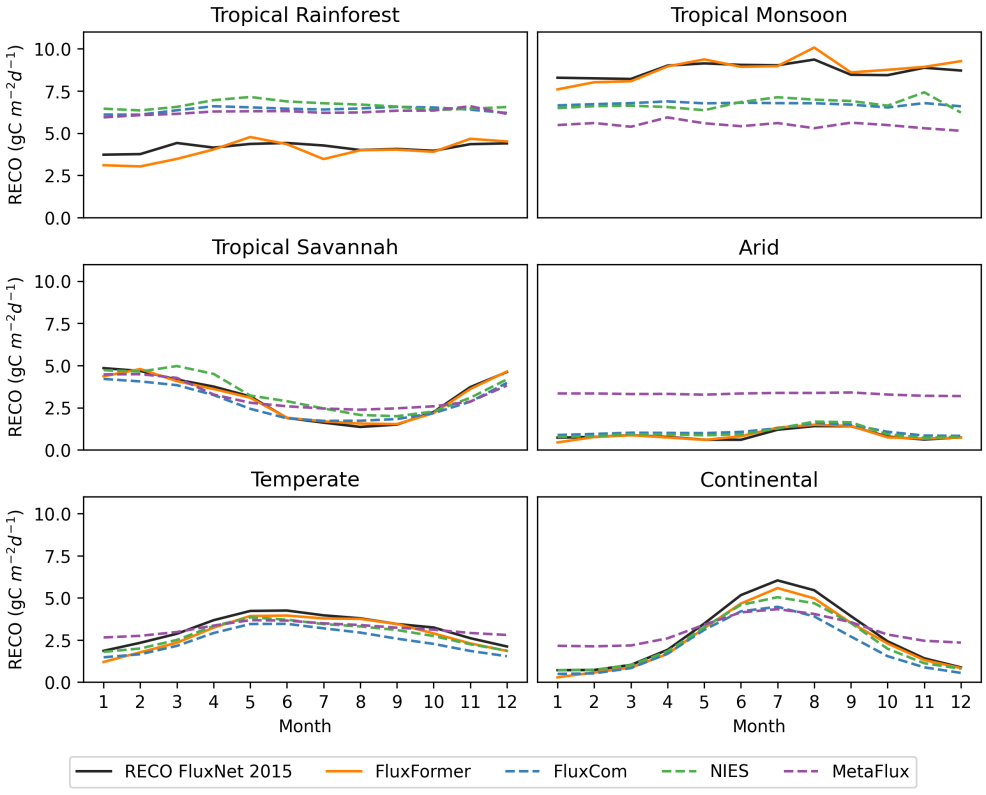

(b) RECO

Figure 4: Seasonality validation with FLUXNET 2015: GPP (a) RECO (b)

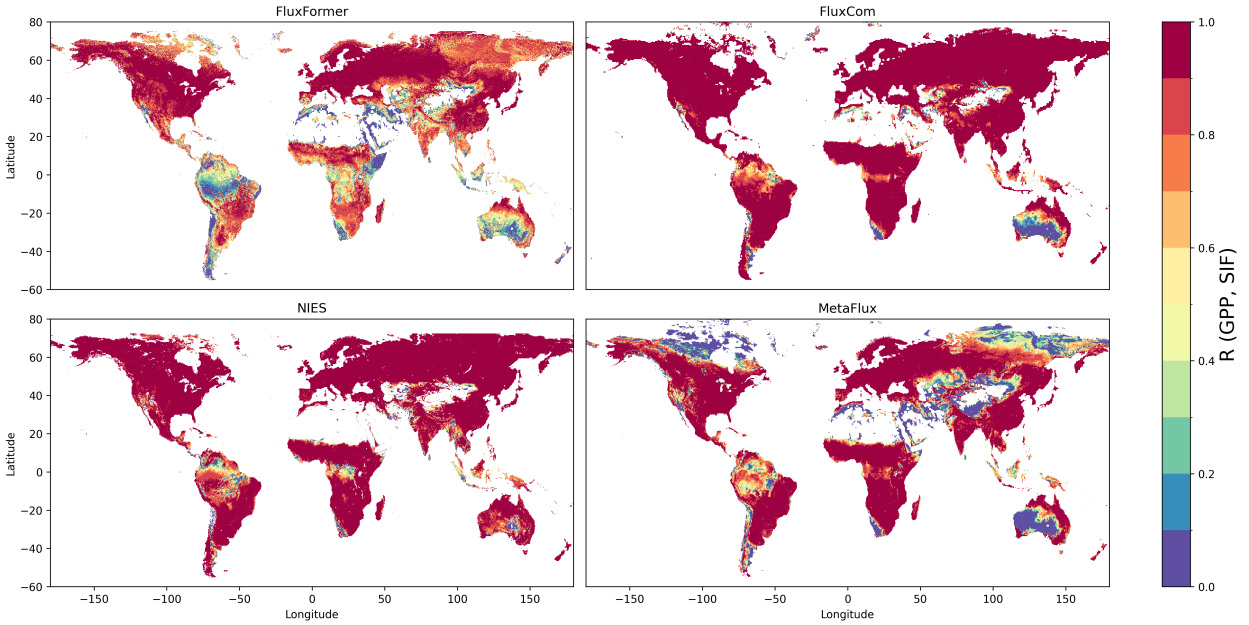

(a) CSIF

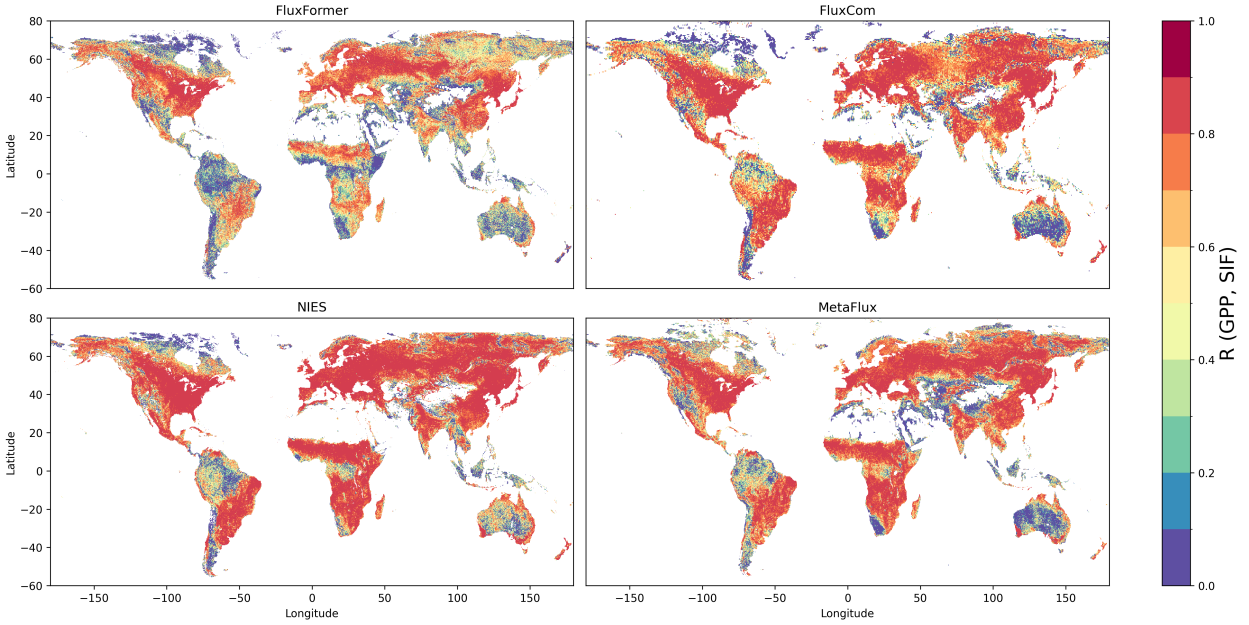

(b) TROPOMI SIF

Figure 5: Validation with SIF products: CSIF (a) TROPOMI SIF (b)

arid regions compared to FLUXCOM, NIES, and MetaFlux. This finding aligns with [Sanders et al., 2016], indicating weaker seasonality in these regions.

4.3 Interannual variations between products

4.3.1 Interannual trend

The interannual trends of FluxFormer and other products (FLUXCOM, NIES, and MetaFlux) are illustrated in Figure 6a. We examined the global annual time series from 2001 to 2019 to analyze the trend in GPP. Our dataset exhibits the highest positive trend, with a growth rate of 0.45 PgC/year. The second-highest trend is observed in the NIES

global annual time series, with a growth rate of 0.32 PgC/year. MetaFlux shows a small increasing trend, albeit with an insignificant p-value of 0.08. On the other hand, FLUXCOM indicates a small negative trend, with a reduction rate of 0.04 PgC per year.

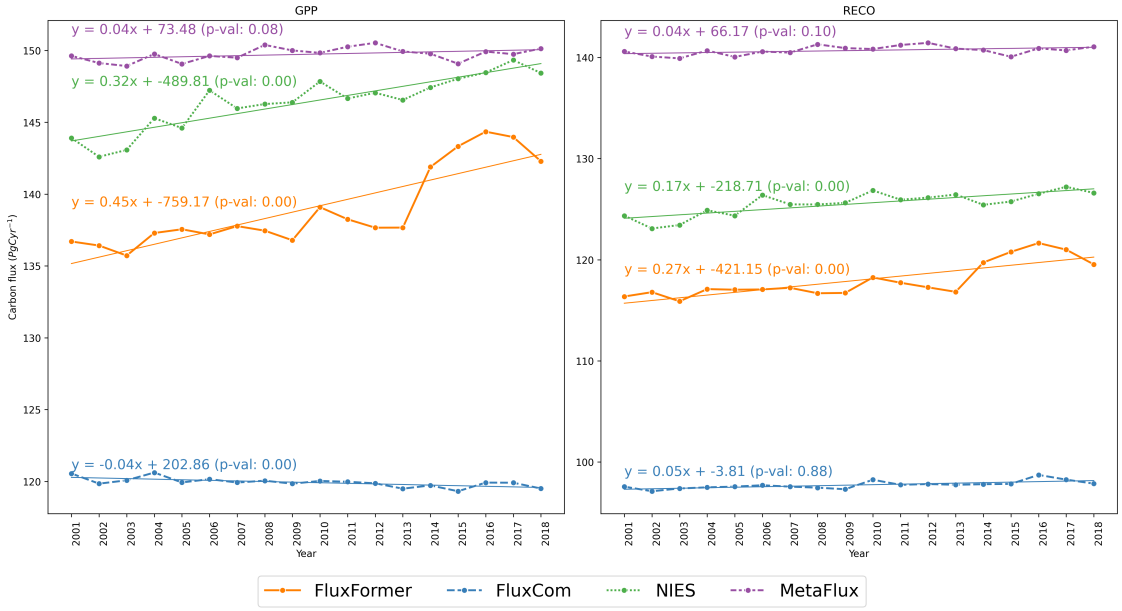

(a) Long term trend of global annual mean GPP and RECO from 2001 to 2019

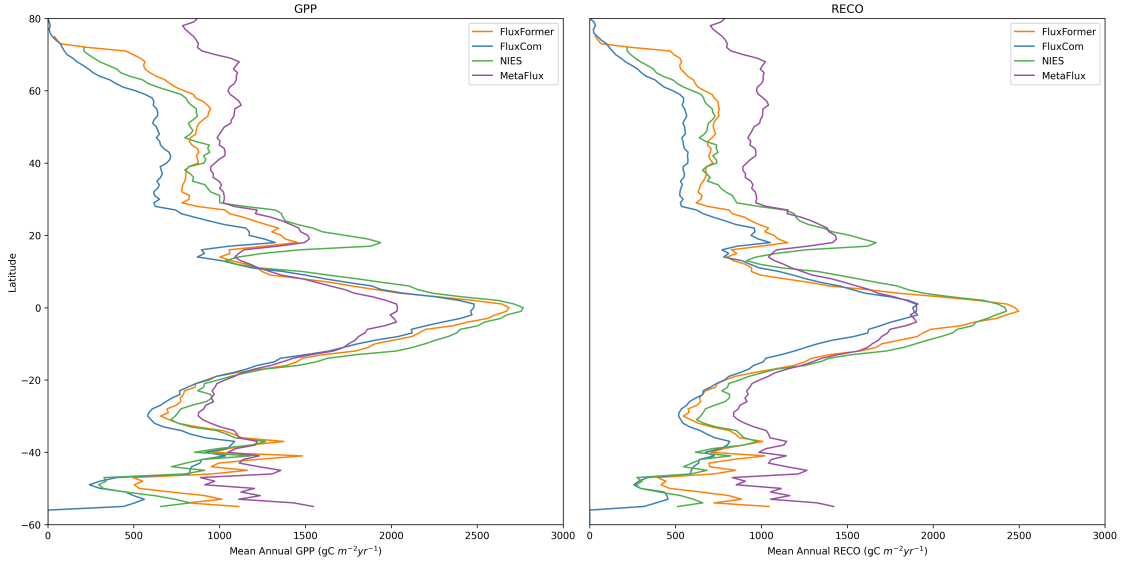

(b) Latitudinal distribution of GPP and RECO

Figure 6: (a) Long term trend and (b) latitudinal distribution of GPP and RECO

Our long-term GPP trend aligns with the expected increase due to the CO_2 fertilization effect, anticipated to enhance the land carbon sink [Piao et al., 2020, Guo et al., 2023, Yang et al., 2022].

We also inspect the latitudinal distribution of GPP and RECO as depicted in Figure 6b. All four products exhibit a gradual increase in both GPP and RECO values from cold climate regions to warm and humid climates in temperate and tropical regions.

4.3.2 Interannual variations

Finally, we assess the interannual variations of GPP and RECO, as illustrated in Figures 7a and 7b, respectively. We observe that our data exhibits lower interannual variability than NIES in desert regions, including Australia, Central Asia, Central America, and South America. We posit that our data may be more reasonable, considering that in desert areas, GPP is expected to be extremely low [Hadley and Szarek, 1981]. Additionally, our dataset demonstrates smaller interannual variability than NIES in the northern parts of Eurasia and North America.

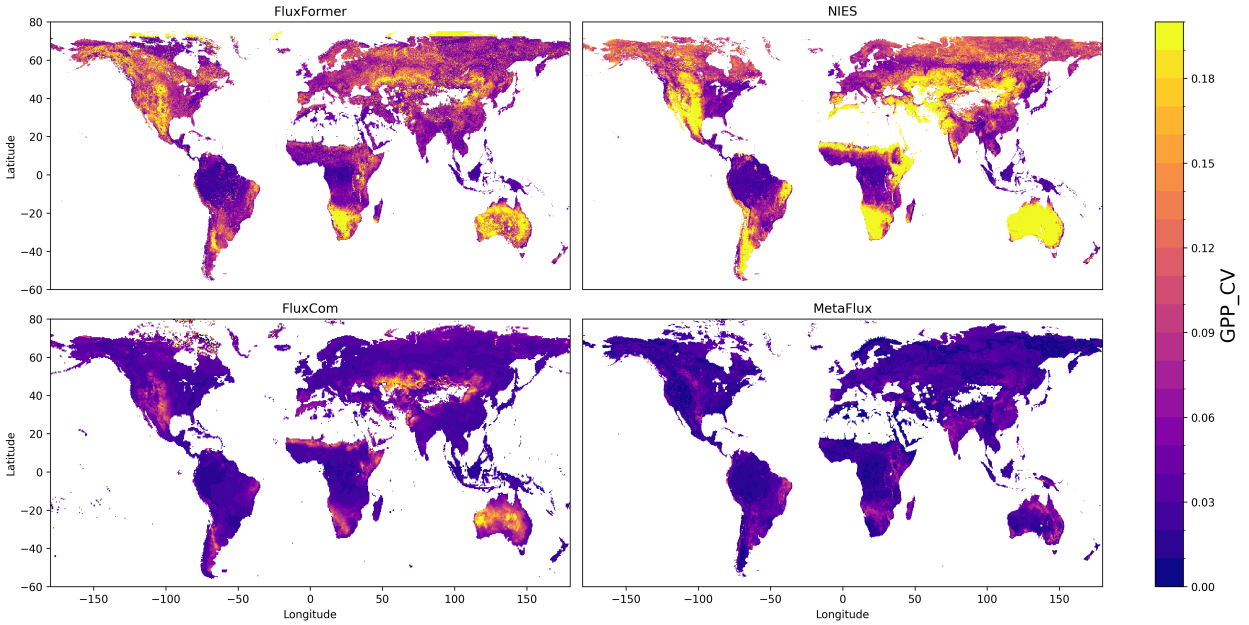

(a) GPP

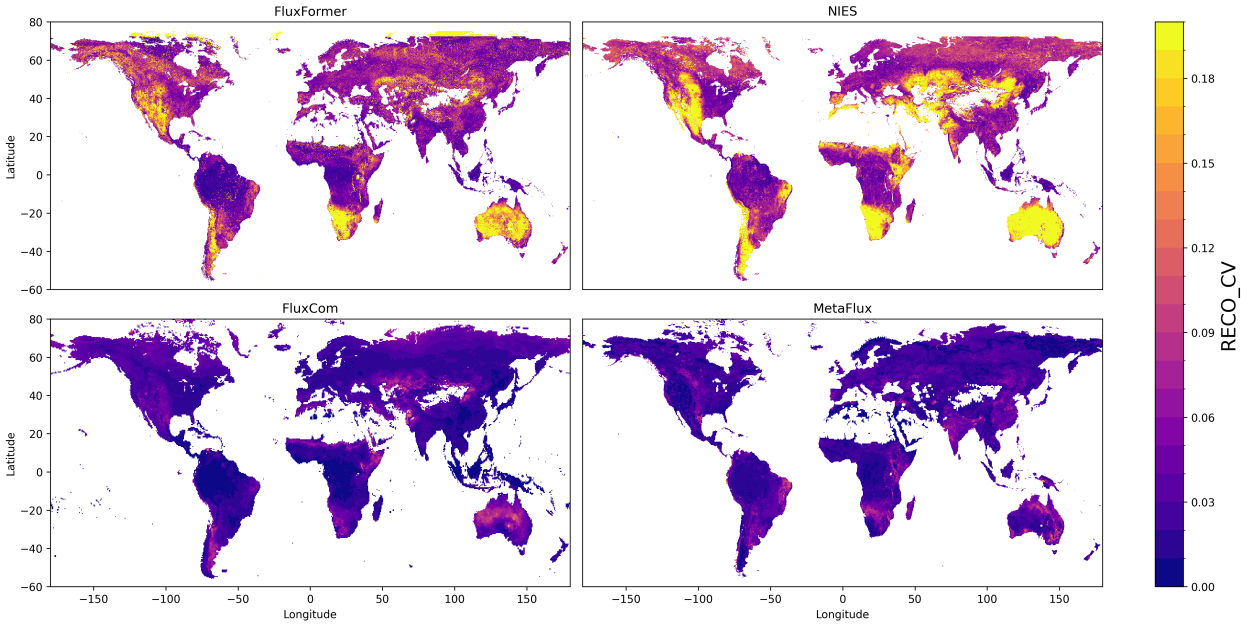

(b) RECO

Figure 7: Interannual variations: GPP (a) RECO (b)

Our dataset displays greater interannual variability compared to FLUXCOM and MetaFlux. This difference could be attributed to the use of distinct remote sensing data sources for upscaling carbon fluxes. Specifically, we employed

LAI and FAPAR from SPOT/VEGETATION and PROBA-V, which aligns with the approach described in [Zeng et al., 2020]. In contrast, FLUXCOM and MetaFlux utilize input remote sensing data sourced from MODIS [Jung et al., 2019, Nathaniel et al., 2023].

5 Conclusion

In this section, we present our work in upscaling global gross primary production and ecosystem respiration. This is achieved through the application of a multivariate timeseries transformer [Zerveas et al., 2021] in conjunction with updated plant functional types data [Harper et al., 2022]. We provide monthly global data for GPP and RECO at a spatial resolution of $0.25° \times 0.25°$, covering the period from 1990 to 2019.

Our data shows improvement with increased correlation and reduced error when compared to FLUXNET 2015 data at both the site level and seasonal trends, outperforming FLUXCOM, NIES, and MetaFlux datasets. Particularly noteworthy is our data's strong correlation with the GPP seasonal trend in the tropical monsoon region ($R = 0.84$), whereas FLUXCOM and MetaFlux exhibit no correlation with the ground measurements seasonal trend in that area.

We further assess the seasonal trend of our dataset using two SIF products, CSIF and TROPOMI SIF. Our dataset exhibits a strong correlation in cold and temperate regions, consistent with other datasets. However, in tropical and semi-arid regions, our dataset shows a lower correlation compared to others, a finding in line with [Sanders et al., 2016]. This lower correlation is attributed to the weak seasonality of GPP in tropical regions and the high complexity of PFTs [Montgomery and Chazdon, 2001], making the linear relationship less evident.

We also investigated the long-term trends of GPP and RECO from 2001 to 2019 and observed that our data exhibits the highest positive trend in GPP during this period, with a growth rate of 0.45 PgC per year. This finding aligns with studies such as [Piao et al., 2020, Guo et al., 2023, Yang et al., 2022], supporting the assumption that the CO_2 fertilization effect should increase GPP over time. In contrast, MetaFlux and the widely used product FLUXCOM fail to replicate the long-term trend of GPP, contradicting the currently recognized significant greening observed from regional to global scales [Piao et al., 2020].

Lastly, we scrutinize the interannual variations of our products in comparison with other datasets. We note that our dataset exhibits lower variations in extreme-low-GPP regions, such as deserts and semi-arid regions, when utilizing the same source of remote sensing data as NIES. However, our dataset shows higher variations than FLUXCOM and MetaFlux, possibly attributable to the utilization of different remote sensing resources.

References

Jia Bai, Helin Zhang, Rui Sun, Xing Li, Jingfeng Xiao, and Yan Wang. Estimation of global gpp from gome-2 and oco-2 sif by considering the dynamic variations of gpp-sif relationship. *Agricultural and Forest Meteorology*, 326: 109180, 2022.

Christian Beer, Markus Reichstein, Enrico Tomelleri, Philippe Ciais, Martin Jung, Nuno Carvalhais, Christian Rödenbeck, M Altaf Arain, Dennis Baldocchi, Gordon B Bonan, et al. Terrestrial gross carbon dioxide uptake: global distribution and covariation with climate. *Science*, 329(5993):834–838, 2010.

Anping Chen, Jiafu Mao, Daniel Ricciuto, Dan Lu, Jingfeng Xiao, Xing Li, Peter E Thornton, and Alan K Knapp. Seasonal changes in gpp/sif ratios and their climatic determinants across the northern hemisphere. *Global Change Biology*, 27(20):5186–5197, 2021.

Min Chen, Rashid Rafique, Ghassem R Asrar, Ben Bond-Lamberty, Philippe Ciais, Fang Zhao, Christopher PO Reyer, Sebastian Ostberg, Jinfeng Chang, Akihiko Ito, et al. Regional contribution to variability and trends of global gross primary productivity. *Environmental Research Letters*, 12(10):105005, 2017.

Russell Doughty, Xiangming Xiao, Philipp Köhler, Christian Frankenberg, Yuanwei Qin, Xiaocui Wu, Shuang Ma, and Berrien Moore III. Global-scale consistency of spaceborne vegetation indices, chlorophyll fluorescence, and photosynthesis. *Journal of Geophysical Research: Biogeosciences*, 126(6):e2020JG006136, 2021.

Mark A Friedl, Damien Sulla-Menashe, Bin Tan, Annemarie Schneider, Navin Ramankutty, Adam Sibley, and Xiaoman Huang. Modis collection 5 global land cover: Algorithm refinements and characterization of new datasets. *Remote sensing of Environment*, 114(1):168–182, 2010.

Pierre Friedlingstein, Michael O'sullivan, Matthew W Jones, Robbie M Andrew, Judith Hauck, Are Olsen, Glen P Peters, Wouter Peters, Julia Pongratz, Stephen Sitch, et al. Global carbon budget 2020. *Earth System Science Data Discussions*, 2020:1–3, 2020.

Lianhong Gu, Jimei Han, Jeffrey D Wood, Christine Y-Y Chang, and Ying Sun. Sun-induced chl fluorescence and its importance for biophysical modeling of photosynthesis based on light reactions. *New Phytologist*, 223(3):1179–1191, 2019.

Luis Guanter, Christian Frankenberg, Anu Dudhia, Philip E Lewis, José Gómez-Dans, Akihiko Kuze, Hiroshi Suto, and Roy G Grainger. Retrieval and global assessment of terrestrial chlorophyll fluorescence from gosat space measurements. *Remote Sensing of Environment*, 121:236–251, 2012.

Renjie Guo, Tiexi Chen, Xin Chen, Wenping Yuan, Shuci Liu, Bin He, Lin Li, Shengzhen Wang, Ting Hu, Qingyun Yan, et al. Estimating global gpp from the plant functional type perspective using a machine learning approach. *Journal of Geophysical Research: Biogeosciences*, page e2022JG007100, 2023.

Neil F Hadley and Stan R Szarek. Productivity of desert ecosystems. *BioScience*, 31(10):747–753, 1981.

Kandice L Harper, Céline Lamarche, Andrew Hartley, Philippe Peylin, Catherine Ottlé, Vladislav Bastrikov, Rodrigo San Martín, Sylvia I Bohnenstengel, Grit Kirches, Martin Boettcher, et al. A 29-year time series of annual 300-metre resolution plant functional type maps for climate models. *Earth System Science Data Discussions*, 2022:1–37, 2022.

Hans Hersbach, Bill Bell, Paul Berrisford, Shoji Hirahara, András Horányi, Joaquín Muñoz-Sabater, Julien Nicolas, Carole Peubey, Raluca Radu, Dinand Schepers, et al. The era5 global reanalysis. *Quarterly Journal of the Royal Meteorological Society*, 146(730):1999–2049, 2020.

M. Jung, C. Schwalm, M. Migliavacca, S. Walther, G. Camps-Valls, S. Koirala, P. Anthoni, S. Besnard, P. Bodesheim, N. Carvalhais, F. Chevallier, F. Gans, D. S. Goll, V. Haverd, P. Köhler, K. Ichii, A. K. Jain, J. Liu, D. Lombardozzi, J. E. M. S. Nabel, J. A. Nelson, M. O'Sullivan, M. Pallandt, D. Papale, W. Peters, J. Pongratz, C. Rödenbeck, S. Sitch, G. Tramontana, A. Walker, U. Weber, and M. Reichstein. Scaling carbon fluxes from eddy covariance sites to globe: synthesis and evaluation of the fluxcom approach. *Biogeosciences*, 17(5):1343–1365, 2020. doi:10.5194/bg-17-1343-2020. URL `https://bg.copernicus.org/articles/17/1343/2020/`.

Martin Jung, Sujan Koirala, Ulrich Weber, Kazuhito Ichii, Fabian Gans, Gustau Camps-Valls, Dario Papale, Christopher Schwalm, Gianluca Tramontana, and Markus Reichstein. The fluxcom ensemble of global land-atmosphere energy fluxes. *Scientific data*, 6(1):74, 2019.

Philipp Köhler, Christian Frankenberg, Troy S Magney, Luis Guanter, Joanna Joiner, and Jochen Landgraf. Global retrievals of solar-induced chlorophyll fluorescence with tropomi: First results and intersensor comparison to oco-2. *Geophysical Research Letters*, 45(19):10–456, 2018.

Corinne Le Quéré, Robbie M Andrew, Pierre Friedlingstein, Stephen Sitch, Judith Hauck, Julia Pongratz, Penelope Pickers, Jan Ivar Korsbakken, Glen P Peters, Josep G Canadell, et al. Global carbon budget 2018. *Earth System Science Data Discussions*, 2018:1–3, 2018.

Shangrong Lin, Jing Li, Qinhuo Liu, Beniamino Gioli, Eugenie Paul-Limoges, Nina Buchmann, Mana Gharun, Lukas Hörtnagl, Lenka Foltỳnová, Jiří Dušek, et al. Improved global estimations of gross primary productivity of natural vegetation types by incorporating plant functional type. *International Journal of Applied Earth Observation and Geoinformation*, 100:102328, 2021.

Xinjie Liu, Liangyun Liu, Jiaochan Hu, Jian Guo, and Shanshan Du. Improving the potential of red sif for estimating gpp by downscaling from the canopy level to the photosystem level. *Agricultural and Forest Meteorology*, 281: 107846, 2020.

Rebecca A Montgomery and Robin L Chazdon. Forest structure, canopy architecture, and light transmittance in tropical wet forests. *Ecology*, 82(10):2707–2718, 2001.

Juan Nathaniel, Jiangong Liu, and Pierre Gentine. Metaflux: Meta-learning global carbon fluxes from sparse spatiotemporal observations. *Scientific Data*, 10(1):440, 2023.

Alexander J Norton, Peter J Rayner, Ernest N Koffi, Marko Scholze, Jeremy D Silver, and Ying-Ping Wang. Estimating global gross primary productivity using chlorophyll fluorescence and a data assimilation system with the bethy-scope model. *Biogeosciences*, 16(15):3069–3093, 2019.

Yude Pan, Richard A Birdsey, Jingyun Fang, Richard Houghton, Pekka E Kauppi, Werner A Kurz, Oliver L Phillips, Anatoly Shvidenko, Simon L Lewis, Josep G Canadell, et al. A large and persistent carbon sink in the world's forests. *Science*, 333(6045):988–993, 2011.

Gilberto Pastorello, Carlo Trotta, Eleonora Canfora, Housen Chu, Danielle Christianson, You-Wei Cheah, Cristina Poindexter, Jiquan Chen, Abdelrahman Elbashandy, Marty Humphrey, et al. The fluxnet2015 dataset and the oneflux processing pipeline for eddy covariance data. *Scientific data*, 7(1):225, 2020.

Shilong Piao, Xuhui Wang, Taejin Park, Chi Chen, XU Lian, Yue He, Jarle W Bjerke, Anping Chen, Philippe Ciais, Hans Tømmervik, et al. Characteristics, drivers and feedbacks of global greening. *Nature Reviews Earth & Environment*, 1 (1):14–27, 2020.

B Poulter, P Ciais, E Hodson, H Lischke, F Maignan, S Plummer, and NE Zimmermann. Plant functional type mapping for earth system models. *Geoscientific Model Development*, 4(4):993–1010, 2011.

Ben Poulter, Natasha MacBean, Andrew Hartley, Iryna Khlystova, Olivier Arino, Richard Betts, Sophie Bontemps, Martin Boettcher, Carsten Brockmann, Pierre Defourny, et al. Plant functional type classification for earth system models: results from the european space agency's land cover climate change initiative. *Geoscientific Model Development*, 8(7):2315–2328, 2015.

Benjamin Poulter, David Frank, Philippe Ciais, Ranga B Myneni, Niels Andela, Jian Bi, Gregoire Broquet, Josep G Canadell, Frederic Chevallier, Yi Y Liu, et al. Contribution of semi-arid ecosystems to interannual variability of the global carbon cycle. *Nature*, 509(7502):600–603, 2014.

Abram FJ Sanders, Willem W Verstraeten, Maurits L Kooreman, Thomas C Van Leth, Jason Beringer, and Joanna Joiner. Spaceborne sun-induced vegetation fluorescence time series from 2007 to 2015 evaluated with australian flux tower measurements. *Remote Sensing*, 8(11):895, 2016.

Stephen Sitch, Pierre Friedlingstein, Nicolas Gruber, Steve D Jones, Guillermo Murray-Tortarolo, Anders Ahlström, Scott C Doney, H Graven, Christoph Heinze, Chris Huntingford, et al. Recent trends and drivers of regional sources and sinks of carbon dioxide. *Biogeosciences*, 12(3):653–679, 2015.

Gianluca Tramontana, Martin Jung, Christopher R Schwalm, Kazuhito Ichii, Gustau Camps-Valls, Botond Ráduly, Markus Reichstein, M Altaf Arain, Alessandro Cescatti, Gerard Kiely, et al. Predicting carbon dioxide and energy fluxes across global fluxnet sites with regression algorithms. *Biogeosciences*, 13(14):4291–4313, 2016.

Ashish Vaswani, Noam Shazeer, Niki Parmar, Jakob Uszkoreit, Llion Jones, Aidan N Gomez, Łukasz Kaiser, and Illia Polosukhin. Attention is all you need. *Advances in neural information processing systems*, 30, 2017.

Aleixandre Verger, Frédéric Baret, and Marie Weiss. Near real-time vegetation monitoring at global scale. *IEEE Journal of Selected Topics in Applied Earth Observations and Remote Sensing*, 7(8):3473–3481, 2014.

You-Ren Wang, Nina Buchmann, Dag O Hessen, Frode Stordal, Jan Willem Erisman, Ane Victoria Vollsnes, Tom Andersen, and Han Dolman. Disentangling effects of natural and anthropogenic drivers on forest net ecosystem production. *Science of the Total Environment*, 839:156326, 2022.

Haixu Wu, Jiehui Xu, Jianmin Wang, and Mingsheng Long. Autoformer: Decomposition transformers with auto-correlation for long-term series forecasting. *Advances in Neural Information Processing Systems*, 34:22419–22430, 2021.

Jingfeng Xiao, Xing Li, Binbin He, M Altaf Arain, Jason Beringer, Ankur R Desai, Carmen Emmel, David Y Hollinger, Alisa Krasnova, Ivan Mammarella, et al. Solar-induced chlorophyll fluorescence exhibits a universal relationship with gross primary productivity across a wide variety of biomes. *Global change biology*, 25(4):e4–e6, 2019.

Liang Xu, Sassan S Saatchi, Yan Yang, Ranga B Myneni, Christian Frankenberg, Diya Chowdhury, and Jian Bi. Satellite observation of tropical forest seasonality: spatial patterns of carbon exchange in amazonia. *Environmental Research Letters*, 10(8):084005, 2015.

Pu Yan, Nianpeng He, Kailiang Yu, Li Xu, and Koenraad Van Meerbeek. Integrating multiple plant functional traits to predict ecosystem productivity. *Communications Biology*, 6(1):239, 2023.

Hualei Yang, Xi Yang, Yongguang Zhang, Mary A Heskel, Xiaoliang Lu, J William Munger, Shucun Sun, and Jianwu Tang. Chlorophyll fluorescence tracks seasonal variations of photosynthesis from leaf to canopy in a temperate forest. *Global Change Biology*, 23(7):2874–2886, 2017.

Ruqi Yang, Jun Wang, Ning Zeng, Stephen Sitch, Wenhan Tang, Matthew Joseph McGrath, Qixiang Cai, Di Liu, Danica Lombardozzi, Hanqin Tian, et al. Divergent historical gpp trends among state-of-the-art multi-model simulations and satellite-based products. *Earth System Dynamics*, 13(2):833–849, 2022.

Jiye Zeng, Tsuneo Matsunaga, Zheng-Hong Tan, Nobuko Saigusa, Tomoko Shirai, Yanhong Tang, Shushi Peng, and Yoko Fukuda. Global terrestrial carbon fluxes of 1999–2019 estimated by upscaling eddy covariance data with a random forest. *Scientific data*, 7(1):313, 2020.

George Zerveas, Srideepika Jayaraman, Dhaval Patel, Anuradha Bhamidipaty, and Carsten Eickhoff. A transformer-based framework for multivariate time series representation learning. In *Proceedings of the 27th ACM SIGKDD conference on knowledge discovery & data mining*, pages 2114–2124, 2021.

Yao Zhang, Joanna Joiner, Seyed Hamed Alemohammad, Sha Zhou, and Pierre Gentine. A global spatially contiguous solar-induced fluorescence (csif) dataset using neural networks. *Biogeosciences*, 15(19):5779–5800, 2018.

Yongguang Zhang, Luis Guanter, Joseph A Berry, Christiaan van der Tol, Xi Yang, Jianwu Tang, and Fangmin Zhang. Model-based analysis of the relationship between sun-induced chlorophyll fluorescence and gross primary production for remote sensing applications. *Remote Sensing of Environment*, 187:145–155, 2016.

Haoyi Zhou, Shanghang Zhang, Jieqi Peng, Shuai Zhang, Jianxin Li, Hui Xiong, and Wancai Zhang. Informer: Beyond efficient transformer for long sequence time-series forecasting. In *Proceedings of the AAAI conference on artificial intelligence*, volume 35, pages 11106–11115, 2021.

Tian Zhou, Ziqing Ma, Qingsong Wen, Xue Wang, Liang Sun, and Rong Jin. Fedformer: Frequency enhanced decomposed transformer for long-term series forecasting. In *International Conference on Machine Learning*, pages 27268–27286. PMLR, 2022.